



HAL
open science

Action pattern of fusarium moniliforme endopolygalacturonase towards pectin fragments: comprehension and prediction

Gwenaëlle André-Leroux, D. Tessier, Estelle Bonnin

► **To cite this version:**

Gwenaëlle André-Leroux, D. Tessier, Estelle Bonnin. Action pattern of fusarium moniliforme endopolygalacturonase towards pectin fragments: comprehension and prediction. *Biochimica et Biophysica Acta Proteins and Proteomics*, 2005, 1749 (1), pp.53-64. 10.1016/j.bbapap.2005.02.008 . hal-02680584

HAL Id: hal-02680584

<https://hal.inrae.fr/hal-02680584>

Submitted on 31 May 2020

HAL is a multi-disciplinary open access archive for the deposit and dissemination of scientific research documents, whether they are published or not. The documents may come from teaching and research institutions in France or abroad, or from public or private research centers.

L'archive ouverte pluridisciplinaire **HAL**, est destinée au dépôt et à la diffusion de documents scientifiques de niveau recherche, publiés ou non, émanant des établissements d'enseignement et de recherche français ou étrangers, des laboratoires publics ou privés.

Copyright

Action pattern of *Fusarium moniliforme* endopolygalacturonase towards pectin fragments: Comprehension and prediction

G. André-Leroux^a, D. Tessier^b, E. Bonnin^{b,*}

^aInstitut Pasteur, Unité de Biochimie Structurale, 25 rue du Dr Roux 75724 Paris Cedex 15, France

^bInstitut National de la Recherche Agronomique, Site de la Géraudière, BP 71624, 44316 Nantes Cedex 3, France

Received 14 September 2004; received in revised form 21 January 2005; accepted 11 February 2005

Available online 9 March 2005

Abstract

The structures of complexes of *Fusarium moniliforme* endopolygalacturonase (endoPG) with non-methylated or partly methylated homogalacturonan fragments were modeled to identify the residues involved in substrate binding and to correlate the cleavage pattern with the experimental productive modes. The conformational space of the complex was extensively explored and malto- to hexo-oligogalacturonates were modeled in the active cleft. To select the most highly probable productive complex for each oligomer between DP2 and 6, four energetic criteria were defined. Noteworthy, the results were in accordance with the experimental results showing the mode of action of this enzyme towards un-methyl-esterified oligogalacturonates. Furthermore, the amino-acid residues involved in the binding were confirmed by similar studies performed on other endoPGs. Then, the oligomers were gradually methyl-esterified at one or more positions and similar docking experiments were carried out. Markedly, the docking energies were not significantly modified by the methyl-esterification of the substrate and it is likely that the methyl-esterification of the substrate does not alter the mode of action of the enzyme. Finally, 1D sequence and 3D structure of the endopolygalacturonase of *Aspergillus niger* II, known to be strictly non-tolerant to methyl-esters, were compared with the sequence and structure of the tolerant *F. moniliforme* endopolygalacturonase to get to a structural comprehension of the tolerant–or not–behaviour of endoPGs with methyl-esterified pectins.

© 2005 Elsevier B.V. All rights reserved.

Keywords: Endopolygalacturonase; Homogalacturonan; Action pattern; Molecular modeling; Subsite binding

1. Introduction

The homogalacturonan constitutes the “smooth” region of pectins that are one of the main polysaccharide of middle lamella and primary cell walls in higher plants. It contains mainly galacturonic acid (GalA) that may be methyl-esterified on the carboxylic group. The degree of methylation (DM) is defined as the percentage of carboxyl groups esterified with methanol. In native pectins, DM can be often up to 70–80%. The homogalacturonan is the best substrate for most of the endopolygalacturonases (endoPGs). Basically, endopolygalacturonases (poly [1,4- α -D-galacturonide]

glycano-hydrolase, EC 3.2.1.15) hydrolyse 1–4 linkages between two GalA residues [1]. They are widely distributed in plants, fungi, yeasts, and bacteria [2] and are the subject of a thorough research including reviews for their purification, properties, and mode of action [3,4]. Based on their sequences and their structurally related catalytic folding, endoPGs have been classified in the family 28 of glycosyl hydrolases, GH28 [5] (<http://www.afmb.cnrs-mrs.fr/CAZY/>). Since most of them follow a similar mechanism of “inverting” enzymes, it could be hypothesised that most endoPGs follow a similar stereochemistry of the hydrolysis reaction with an inversion of the configuration in the cleaved substrate [6]. Their activity is highly dependant on the DM of the substrate and often decreases with an increasing DM [7,8]. In that sense, the combined activity of endoPG and pectin methylesterase (PME) is necessary to extensively

* Corresponding author.

E-mail address: gandre@pasteur.fr (E. Bonnin).

Table 1
Tolerance to methyl-esterified substrates

Enzyme	SwissProt (pdb)	DM of the best substrate	% identity (HSSP)
<i>F. moniliforme</i>	Q07181 (1hg8)	Up to 45 [12]	
<i>A. niger</i>			
PG D	Q9P4W2	0 [9]	63
PG B	Q9P4W3	22 [23]	50
PG A	Q9P4W4	7–22 [23]	48
PG II	P26214 (1czf)	0 [23]	46
PG I	P26213 (1nhc)	0 [8]	43
PG C	Q12554	0–7 [8]	42

Results of HSSP alignment of *F. moniliforme* with *A. niger* PGs. In bold: PGII of *A. niger* was chosen to be compared to *F. moniliforme* PG in the study of the molecular features for the tolerance to methyl-esters.

degrade homogalacturonan. However, some endoPGs exhibit interesting enhanced activity towards slightly methyl-esterified substrates. It is particularly the case for the endoPGA and endoPGB of *Aspergillus niger*, for which the highest specific activity was found for a pectin with DM 22 [9,10]. For the endoPG of *Verticillium albo-atrum*, another fungal plant pathogen which causes wilt in tomatoes [11], the best substrate was a 56% methyl-esterified pectin [12]. On the opposite, endoPGII from *A. niger* was shown to preferentially hydrolyse polygalacturonic acid and not to be tolerant towards methyl groups as its relative specific activity towards pectin with DM 7 was 68% of that to polygalacturonic acid [8] (Table 1).

In previous papers, a detailed study of the endoPG of *Fusarium moniliforme* reported its purification and experimentally determined mode of action towards both GalA oligomers [13] and methyl-esterified pectins [14]. In the present paper, molecular modeling was combined with bioinformatics to understand the conformational behaviour of homogalacturonan fragments inside the active site as well as the docking affinity of *F. moniliforme* endoPG. Structural features were indeed found relevant for a DM varying from 0 to 66% and a degree of polymerization (DP) from 2 to 6. The results are discussed in the light of two previous elegant papers using computer modeling on *Aspergillus aculeatus* polygalacturonase and rhamnogalacturonase [15,16]. Finally, the ultimate goal of this study was to predict the docking behaviour of mono and multi-methyl-esterified substrates as well as the cleavage pattern of *F. moniliforme* endoPG.

2. Materials and methods

2.1. Molecular modeling

Molecular modeling was carried out on Silicon Graphics computers with the Accelrys packages (Accelrys, Inc, San Diego, CA, USA). Molecular displays and energy minimisations were performed with InsightII, combining Biopolymer and Discover modules. For all calculations,

the CFF91 force field with the steepest descent minimisation was selected. This force field has been proved to be adapted to the protein/polysaccharide interaction studies [17,18]. The oligosaccharide can adopt a large range of flexible conformations from chair to skew, boat or envelope forms due to puckering. In addition, each glycosidic linkage displays rotational degrees of freedom. That is why an exhaustive search in docking an oligosaccharide in the cleft or a protein is computationally formidable and needs some conformational restriction in respect with the authorized flexibility. So, for the sake of CPU time, the backbone of the protein was kept fixed whereas the protein side chains were completely free to move. No constraint was applied on the substrate but the modeling of the study was stepwise as the GalA residues were gradually joined to both reducing and non-reducing ends. Each enzyme/substrate complex was then carefully optimised and relaxed with a long minimisation of 15,000 iterations. We ended up with four energetic criteria; the potential energies of the protein, the substrate, and the complex, plus the docking energy of the complex, which is exclusively the contribution of the residues involved through van der Waals and electrostatic interactions with the oligosaccharide. After a careful selection of the complexes through this set of energetic parameters, the amino-acid residues involved in the subsites were listed and the subsite affinities were carefully measured. The process was repeated until the oligomer completely spanned the active cleft.

2.2. Coordinates of the enzyme

The crystal structure of *F. moniliforme* endopolygalacturonase was determined by X-ray diffraction at 1.73 Å [19]. Such coordinates are very useful in attempting to deduce the catalytic mechanism of the enzyme and have been used as the starting point of our modeling study (1hg8.pdb) (Fig. 1).

2.3. Coordinates of the substrate

2.3.1. Construction of the di-galacturonic acid

The most highly probable conformations of a digalacturonic acid (DP2) are mainly driven by the α -(1,4) glycosidic linkage between the two GalA moieties. The linkage is fully described by the set of (φ, ψ) dihedral angles, respectively the dihedral angles between atoms $O_5-C_1-O_{4'}$ - $C_{4'}$ and $C_1-O_{4'}$ - $C_{4'}$ - $C_{5'}$ of the disaccharide, the prime indicating the reducing end. Those dihedral angles can vary from -180° to $+180^\circ$. Every set of (φ, ψ) dihedral angles corresponds to a given geometry with a potential energy value of the diGalA. A (φ, ψ) map was built, ranging both φ and ψ from -180° to $+180^\circ$. Logically, the conformation that leads to the lowest potential energy was used as the starting disaccharide geometry for the elongation of the substrates inside the cleft of the enzyme.

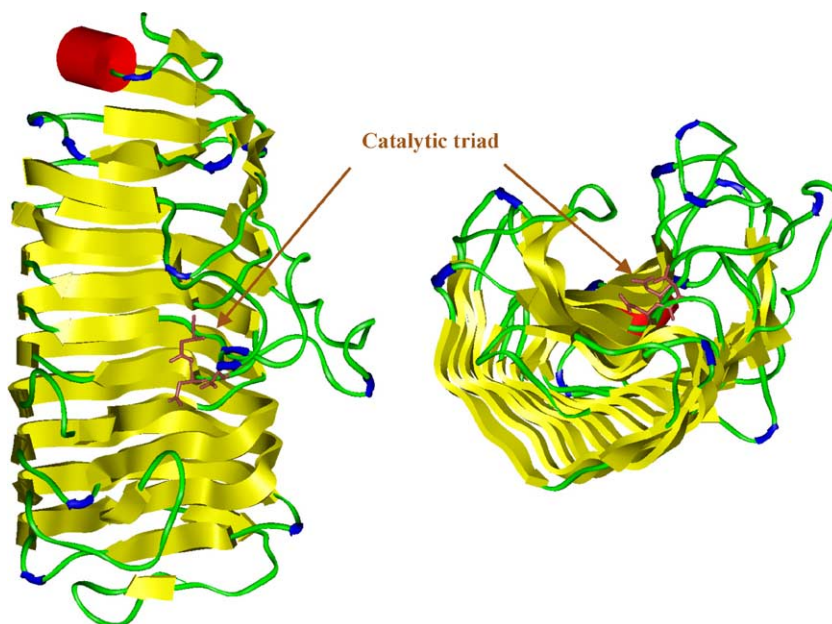


Fig. 1. 1hg8.pdb with the right handed fold highlighted-front and side views.

2.3.2. Elongation of the substrate

The DP2 was manually positioned in the close vicinity of the catalytic triad formed by D191, D212, and D213, so that it spanned subsites -1 and $+1$. The minimisation (description above) optimised the complex. The elongation of the substrate from DP2 to DP3 and, more generally, from DP_n to DP_{n+1} , implied the addition of a supplementary GalA moiety ($n+1$) to the oligosaccharide DP_n docked in the groove. The addition obviously involved a newly formed α -(1,4) glycosidic linkage. Gradually, the additional GalA was bound in respect to the lowest energy of the α -(1,4) dimer. The GalA moiety was each time added to the lowest energy conformation of the previous DP_n fragment, selected after minimisation from the whole set of DP_n geometries. The DP_{n+1} complex was then minimised using the same protocol.

For each oligomer, all the productive binding modes were systematically tested. For example, a DP3 can span subsites -2 , -1 and $+1$ or cover subsites -1 , $+1$ and $+2$. To be more precise, the previous binding modes are shortened respectively to $2/1$ and $1/2$, referring to the distribution of the substrate apart from the catalytic site. Similarly, the binding schemes for DP4, DP5, and DP6 were all tested: respectively $2/2$ vs. $3/1$, $3/2$ vs. $2/3$ and $4/2$ vs. $3/3$ and $2/4$ to be eventually discriminated. Among the DP_n conformations, the selection could not be done, in any case, on the assessment of a single energy value. None of the energy values are pertinent enough to constitute an ultimate criterion of selection. Every value must be taken within its entire energy package and compared to the equivalent energy set of its counterpart in DP for a relevant selection. The complex energy is the sum of the energy of the whole protein plus the entire substrate. The interaction energy, also called the docking energy, can be understood as the strict

contribution of not covalent interaction between the ligand and the protein. It only implies the residues of the protein that are involved in the binding of the sugar. It is an interaction energy corresponding to short distance electrostatic and van der Waals contributions.

2.3.3. Position of the methyl group

To create mono to tetra methyl-esterified oligogalacturonic fragments of DP_n , we started from its un-methyl-esterified homologous DP_n . The four positions of the methyl dihedral angle ω , $C_7-O_6-C_6-C_5$, were systematically tested, so that the low energy dihedral values -180° , 0° , 60° and -60° were minimised. The methylation position was numbered from the reducing end. As a matter of fact, the methyl group of a GalA fragment, positioned at its ultimate reducing end, will always be numbered 1, whatever its docking position. The complex was then minimised within the similar previous procedure.

2.3.4. Bioinformatics

We retrieved primary sequences from the HSSP database (Homology-derived StructureS of Proteins), a derived database merging information from three-dimensional structures and one-dimensional sequences of proteins [20]. We used SRS at the EBI Institute [21]: <http://srs.ebi.ac.uk>. The *F. moniliforme* PDB accession number 1hg8 was used as a query. From the set of endoPG aligned sequences family, we selected the most similar sequences whose tolerance towards methyl-esterified substrates are known. From that result, *F. moniliforme* endoPG and *A. niger* endoPG II were aligned based on their 3D structures, using TCoffee [22]. To be more precise, we did some research to identify the sequence motifs that could be responsible for the pectin docking, i.e., the methylated pectin compared to the pectate (charged homo-

galacturonan), by using PRATT [23] on the following <http://idefix.univ-rennes1.fr:8080/PatternDiscovery> website.

3. Results

3.1. The (φ, ψ) map

The (φ, ψ) map, built for the dimer with the CFF91 force field, evidenced two low energy conformations. They were similar to those found by Di Nola, who used the GROMOS package, especially the reference minimum at $(76^\circ; 114^\circ)$ [24]. The two minima displayed a similar hydrogen bond network compared to the previous study. Noteworthily, by repeating x times the dimeric conformation, we obtained a DP_{2x} right handed 3₁ helix, as found in the native state of homogalacturonan, under sodium form [25,26].

3.2. Complexes with un-methyl-esterified substrates

The distributions of the substrate apart from the cleavage site and the complete set of energy values are compiled in Table 2. The energy repartition, subsite by subsite, was carefully measured to discriminate strong from weak affinity subsites. The values are compiled in Table 3.

As a general trend for this set of data, the cleavage is definitely more probable on the reducing side of the substrate. This is in full agreement with the crystallographic and modeling studies on *A. aculeatus* and *Stereum purpureum* endoPGs [15,27]. The non-reducing end of the ligand points towards the N-terminal end of the enzyme as it was also mentioned previously (Fig. 4 (a), (b)). The general shape of the oligosaccharide displayed neither sensitive distortion of the ⁴C₁ chair conformation nor deformation of the glycosidic linkage from the global minimum. No distorted skew, envelope, or boat conformation was evidenced. Every α -(1,4) glycosidic linkage stayed in its initial minimum energy conformation where the homogalacturonate showed strong redundancy of the native 3₁ helix [24–26]. The protein/oligosaccharide interactions were reinforced: The longer the substrate, the stronger the interaction. Interestingly, the docking interaction started around –55 kcal/mol for a DP2 and increased continuously to –161 kcal/mol for DP6. The docking energy plot versus DP gave a linear curve for DP2 to DP5 with an $R^2=0.9991$, then a plateau at DP6 (data not shown). This feature is in excellent agreement with the experimental results, performed on this enzyme, which showed the kinetic parameters, affinity, and maximum rate of hydrolysis increasing with chain length up to an hexamer for which V_{\max} was in the same range as with homogalacturonan [13]. Besides, with DP6, the substrate fully occupied the active crevice so that another subsite was not likely to dock a supplementary GalA moiety.

For DP2, the docking energy was quite weak, with an energy value of –55 kcal/mol. Even though the docking was sterically possible, the binding was nevertheless not

Table 2

Complex and docking energies for un-methyl-esterified and methyl-esterified oligogalacturonate/PG complexes

Cleavage pattern	Energy		Favoured binding model	Experimental results
	Complex	Docking		
<i>DP2</i>				
G/G	–2197	–55		
M/M	–2158	+88		
<i>DP3</i>				
G/G-G	–2200	–97	****	
G-G/G	–2194	–88		****
<i>DP4</i>				
G-G/G-G	–2219	–116		
G-G-G/G	–2237	–123	****	****
G-M-G/G	–2203	–120		
M-G-G/G	–2198	–125		
M-M-G/G	–2162	–122		
<i>DP5</i>				
G-G/G-G-G	–2229	–118		
G-G-G/G-G	–2259	–147	****	****
G-G-G/G-M	–2231	–144		
G-M-G/G-G	–2225	–144		
M-G-G/G-G	–2220	–149		
G-M-G/G-M	–2196	–143		
M-G-G/G-M	–2191	–147		
M-M-G/G-G	–2184	–146		
M-M-G/G-M	–2155	–145		
<i>DP6</i>				
G-G/G-G-G-G	–2287	–125		
G-G-G/G-G-G	–2277	–147		
G-G-G-G/G-G	–2260	–161	****	****
G-G-G-G/G-M	–2234	–160		
G-G-M-G/G-G	–2209	–168		
G-M-G-G/G-G	–2240	–170		
M-G-G-G/G-G	–2229	–169		
G-G-M-G/G-M	–2181	–167		
G-M-G-G/G-M	–2212	–169		
M-G-G-G/G-M	–2201	–168		
G-M-M-G/G-G	–2186	–171		
M-G-M-G/G-G	–2204	–164		
M-M-G-G/G-G	–2205	–171		
G-M-M-G/G-M	–2158	–170		
M-G-M-G/G-M	–2147	–170		
M-M-G-G/G-M	–2176	–170		
M-M-M-G/G-G	–2151	–173		
M-M-M-G/G-M	–2123	–172		

The favoured binding of non-methylated oligomers exhibit the lowest docking energy values. They are compared with the experimental results given in Bonnin et al. [13]. G indicates a non-methylated residue, M indicates a methylated residue, (-) indicates a linkage, and (/) indicates the cleavage site. Non-methylated and methylated oligomers are separated by a free line for each DP.

**** Evidence the agreement between the experimental work and the molecular modelling data.

favourable. For DP3 ligand, regarding both the docking and the complex potential energies, one should favour the pattern 1/2 vs. 2/1 (respectively –97 vs. –88 kcal/mol) but the energy of the sugar was twice the energy of the sugar

Table 3
Subsite affinities for un-methyl-esterified and methyl-esterified oligogalacturonate/PG complexes

Cleavage pattern	Docking	Energy subsite by subsite						
		−4	−3	−2	−1	+1	+2	+3
<i>DP2</i>								
G/G	−55							
M/M	+88							
<i>DP3</i>								
G/G-G	−97				−40	−33	−29	
G-G/G	−88			−28	−39	−29		
<i>DP4</i>								
G-G/G-G	−116			−28	−35	−31	−29	
G-G-G/G	−123		−46	−21	−32	−29		
G-M-G/G	−120		−44	−22	−31	−29		
M-G-G/G	−125		−49	−23	−31	−29		
M-M-G/G	−122		−47	−23	−31	−29		
<i>DP5</i>								
G-G-G-G-G	−118			−28	−35	−32	−26	−7
G-G-G/G-G	−147		−46	−23	−32	−32	−24	
G-G-G/G-M	−144		−45	−23	−31	−32	−22	
G-M-G/G-G	−144		−44	−23	−31	−32	−24	
M-G-G/G-G	−149		−49	−23	−32	−32	−24	
G-M-G/G-M	−143		−44	−23	−31	−32	−22	
M-G-G/G-M	−147		−49	−23	−32	−32	−23	
M-M-G/G-G	−146		−47	−23	−31	−32	−24	
M-M-G/G-M	−145		−47	−23	−31	−32	−22	
<i>DP6</i>								
G-G-G-G-G-G	−125							
G-G-G/G-G-G	−147		−46	−23	−32	−30	−22	−4
G-G-G-G/G-G	−161	−27	−34	−25	−35	−32	−23	
G-G-G-G/G-M	−160	−30	−32	−25	−35	−32	−21	
G-G-M-G/G-G	−168	−35	−31	−28	−35	−32	−23	
G-M-G-G/G-G	−170	−38	−33	−25	−35	−32	−23	
M-G-G-G/G-G	−169	−38	−32	−25	−35	−32	−23	
G-G-M-G/G-M	−167	−35	−31	−28	−35	−32	−21	
G-M-G-G/G-M	−169	−38	−33	−25	−34	−32	−21	
M-G-G-G/G-M	−168	−38	−32	−25	−35	−32	−21	
G-M-M-G/G-G	−171	−38	−32	−27	−35	−32	−23	
M-G-M-G/G-G	−164	−40	−30	−22	−33	−32	−23	
M-M-G-G/G-G	−171	−40	−31	−25	−34	−32	−23	
G-M-M-G/G-M	−170	−38	−32	−27	−35	−32	−21	
M-G-M-G/G-M	−170	−40	−30	−28	−35	−32	−21	
M-M-G-G/G-M	−170	−40	−32	−25	−34	−32	−21	
M-M-M-G/G-G	−173	−40	−31	−26	−35	−32	−23	
M-M-M-G/G-M	−172	−41	−31	−24	−35	−32	−21	

The nomenclature of oligomers is explained in Table 2 legend. The subsites bearing methylated GalA have their affinity in bold.

in the first 1/2 complex. So it would be extremely hazardous to discriminate the 1/2 from the 2/1 distribution.

The gradual elongation of the substrate favoured the binding patterns: 3/1 vs. 2/2 for DP4, 3/2 vs. 2/3 for DP5, and 4/2 vs. 3/3 or 2/4 for DP6. The energy binding profiles were in excellent agreement with the hydrolysis pattern determined by mass spectrometry for DP4 to DP6 [13]. The bond was preferentially cleaved near the reducing end and the asymmetry of the binding site was confirmed. In addition, subsites −1 and +1 evidenced strong affinity as expected [15,16,27]. The evaluation of the contribution of each subsite explained the asymmetric trend: At DP4,

subsite −3 acted as a much stronger subsite than subsite +2 with a seriously higher affinity for the GalA of −46 kcal/mol vs. −29 kcal/mol (Table 3). Similarly for DP5, the distribution 3/2 vs. 2/3 was largely favoured due to subsite −3 that displayed an affinity of −46 kcal/mol compared to −7 kcal/mol for an hypothetical subsite +3. Besides, for the docking of DP6, the binding pattern was far more favourable for 4/2 (−161.4 kcal/mol) than 3/3 (147.0 kcal/mol) or 2/4 (−125.3 kcal/mol). In details for pattern of 4/2 over 3/3, the affinities for subsites [−2,+2] were strictly comparable, the difference was obvious at the bordering subsites −4 and +3. Subsite +3 (−4 kcal/mol) was too weak

to balance the very strong subsite -4 (-27 kcal/mol). In return, such an affinity pattern evidenced a supplementary subsite at position -4 . With a value of -27 kcal/mol, this subsite displayed a rather strong affinity for GalA, in the same range as subsites -2 and $+2$.

3.3. Complexes with methyl-esterified substrates

Our results for the methyl-esterified complexes are also compiled in Tables 2 and 3. The affinity concerning the methyl-esterified sugar is highlighted in bold in Table 3, so its occupation at definite subsite(s) is visually clear. To select the most probable complex, the set of energy values is similar to the one with no methyl group. The comparison between the given DP_n methyl-esterified conformers obviously implies a similar methylation degree with an identical methyl positioning. Table 3 also compiles the affinity measured subsite by subsite for the methyl-esterified oligoGalA. As a general and expected trend, the enzyme displayed an asymmetric mode of action with a cleavage pattern strictly occurring on the reducing side of the ligand. Thus, the non-reducing end of the ligand pointed towards the N-terminal end of the enzyme (Fig. 5 (a), (b)), as experimentally proved for other endoPGs or rhamnogalacturonases [15,16,27]. The potential energy of the protein was strictly unchanged while the complex and sugar energies decreased with the increasing DM. This was partly due to the additional atoms. In any case, neither the distortion of the sugar ring nor the deformation of the glycosidic linkages occurred, especially at subsites -1 and $+1$ where they were sterically unable to accommodate a methylesterified GalA. Actually, the docking energy for the di-methyl-esterified DP2 was appalling; $+88$ kcal/mol compared to -55 kcal/mol for its un-methyl-esterified reference. In fact, the docking energy was so weak that this complex had reasonably no chance to occur and to be productive.

The methyl-esterification started at DP4. The global interaction binding was deeply reinforced with the length of the substrate as the docking energy increases from -120 kcal/mol for a DP4 to -172 kcal/mol for a DP6. One more time, the longer the substrate, the better the affinity, as evidenced experimentally from the native substrate. The presence of one to several methyl groups did not disrupt the interaction at subsites $+2$, -2 , and -3 . Conversely, it could reinforce the binding as the docking energy was in the same range or even higher than the values observed for un-methyl-esterified oligomers. In more details, the methyl group, docked at subsite $+2$, destabilized very gently the system with a loss of 1 to 4 kcal/mol in the subsite interaction. The influence of a methyl group at subsite -2 depends on the length of the substrate. Noteworthy, subsite -3 , already strong (respectively -46 kcal/mol for the un-methyl-esterified DP4, DP5, and -34 for DP6), got stronger in presence of a methyl group as it reached -49 kcal/mol. Finally, the methyl group at position -4 clearly strengthened the binding of the sugar with an increase in

Table 4

Dihedral values of methyl groups in the methylated oligomers of DP4 to 6

Cleavage pattern	Subsites						
	-4	-3	-2	-1	$+1$	$+2$	$+3$
<i>DP4</i>							
G-M-G/G			-176.4				
M-G-G/G		-17.7					
M-M-G/G		-7.5	-176.2				
<i>DP5</i>							
G-G-G/G-M							179.6
G-M-G/G-G			-175.9				
M-G-G/G-G		-17.2					
G-M-G/G-M			-175.9				-179.5
M-G-G/G-M		-17.3					-179.5
M-M-G/G-G		-6.6	175.8				
M-M-G/G-M		-6.7	-175.8				179.5
<i>DP6</i>							
G-G-G-G/G-M							179.3
G-G-M-G/G-G			-33.4				
G-M-G-G/G-G		179.8					
M-G-G-G/G-G	2.5						
G-G-M-G/G-M			-33.4				179.2
G-M-G-G/G-M		179.8					179.3
M-G-G-G/G-M	2.5						179.3
G-M-M-G/G-G		179.6	-30.4				
M-G-M-G/G-G	0.6		-175.8				
M-M-G-G/G-G	2.4	178.9					
G-M-M-G/G-M		-179.7	-30.3				179.2
M-G-M-G/G-M	0.8		-32.1				179.2
M-M-G-G/G-M	2.5	179.2					179.3
M-M-M-G/G-G	2.3	179.5	-28.8				
M-M-M-G/G-M	2.4	179.2	-28.5				179.2

subsite affinity up to 10 kcal/mol. To illustrate, the un-methyl-esterified DP6 gave -30 kcal/mol when its fourth times methyl-esterified homologous gained 11 kcal/mol to reach -41 kcal/mol (Table 4).

At a dihedral level, among the four dihedral values tested, 180° , 0° and $\pm 60^\circ$, the 180° and 0° values, sometimes drifted to -30° after minimisation, were the most represented. Subsites -4 and $+2$ bound the methyl groups, strictly positioned at respectively 0° and 180° . Subsites -3 and -2 were less stringent as they both tolerated variations around 180° and 0° . In any case, when two consecutive methyl groups occurred on an oligomer, the two dihedral angles were in opposite direction ($0^\circ/180^\circ$ or $180^\circ/0^\circ$).

3.4. Comparison between endoPGs

From the set of endoPG sequences aligned with *F. moniliforme* endoPG, we selected the most similar sequences whose tolerance towards methyl-esterified substrates were known. *F. moniliforme* endoPG displays a tolerance to pectin methyl group up to DM 45% [14], when *A. niger* endoPGII is conversely not tolerant at all for those methyl groups [8]. *A. niger* endoPGII structure has been determined at 1.68 Å [28]. The 1D/3D comparison and the understanding of methyl tolerance will now be focused on.

The HSSP sequence alignment evidenced 46% identity and 63% similarity between those two enzymes (Table 1). Markedly, they could be 3D aligned all along their entire sequence (Fig. 2) with a deviation of less than 1.5 Å between the two backbones (Fig. 3). The only significant difference was located between P163 and P171 where *F. moniliforme* displayed an insertion loop whose sequence is KSGSLPAA which occurred between strands β_{14} and β_{15} . The latter strand contains the highly conserved regions: HNTD where D is one of the catalytic aspartic residues. This structural feature was located on the edge of the catalytic cleft on the reducing end binding side and seemed actually too far from the centre of the reaction to be relevant as to explain the difference in the behaviour of the two enzymes towards the methylated substrates (Fig. 2). Indeed, to understand this difference, the comparison has to be enlarged to the pectin methylesterases (PMEs).

PMEs release methanol from the hydrolysis of the methyl-ester linkages of highly methyl-esterified pectins. They belong to the Carbohydrate Esterase family 8 from CAZY [5]. Interestingly, PME and endoPGs share a similar overall right-handed β -helical structure and can both act on methyl-esterified substrates [15,19,27–32]. Again, to be able

to identify conserved residues or signature motifs that could be responsible for the docking of small hydrophobic methyl groups, the sequences and the 3D structures of PMEs were compared with the sequences and structures of *A. niger* endoPGII and *Fusarium* endoPG. The clustalW comparison displayed neither relevant alignment nor highly conserved residues or consensus motifs (data not shown) as was mentioned previously [32]. With the PRATT software, 15 sequence motifs were identified with a length average of 25 amino-acid residues. Among them, only seven motifs contained a single conserved amino-acid residue, known to be involved in the binding of the homogalacturonan. Moreover, the 3D superimposition between *F. moniliforme* endoPG 1hg8.pdb and PMEs from carrot 1gq8.pdb and *Erwinia chrysantemi* 1qjv.pdb did not evidence any 3D signature for the docking of the methyl groups. In fact, despite a similar backbone folding, a conserved asparagine ladder [31,32], and some consensus amino-acid residues, the 3D structures superimposition was not fully relevant. The strong differences in the loop lengths and locations created a much larger catalytic groove for PMEs and made tricky the superimposition on the subsites of *F. moniliforme* endoPG. Finally, in the PMEs groove, the hydrophobic residues were

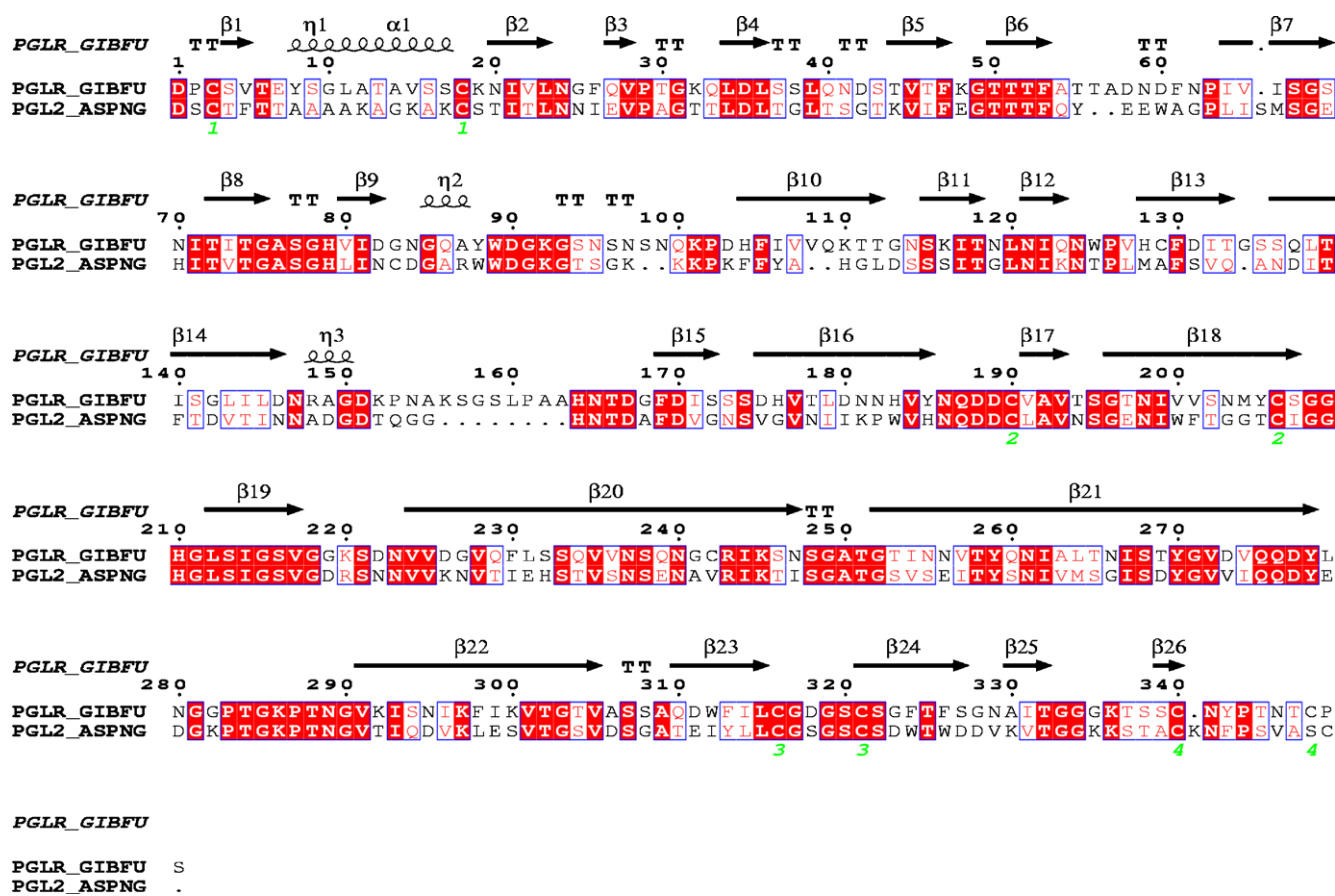


Fig. 2. An amino-acid alignment based on three-dimensional structures of *F. moniliforme* endoPG (PLGR_GIBFU) and *A. niger* endoPG II (PLG2_ASPNG). Arrows above the sequences show right strands. The boxed residues are the residues highly similar; the ones boxed in red are the ones strictly conserved. The boxes are issued from ESPrnt [33]. The 24 amino-acids delta between the PLGR_GIBFU sequence and 1hg8.pdb structure numberings is due to the signal peptide. (For interpretation of the references to colour in this figure legend, the reader is referred to the web version of this article.)

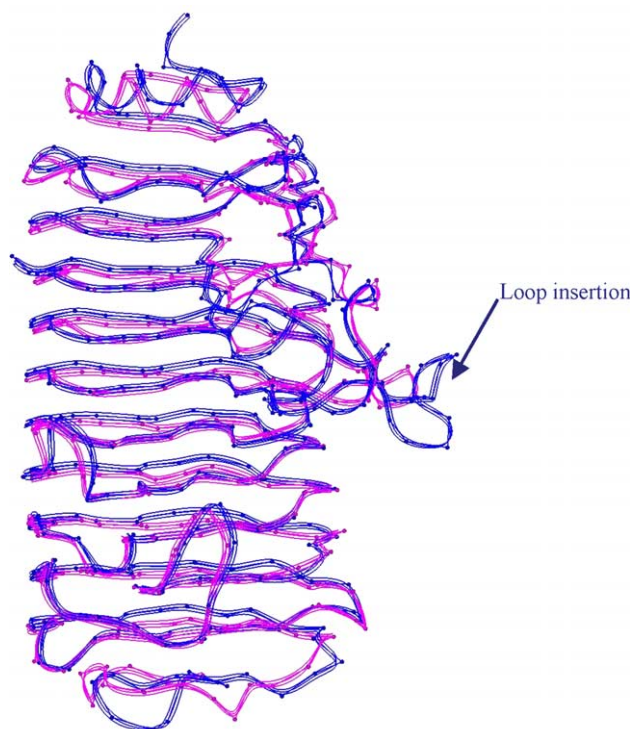


Fig. 3. Superimposition of *F. moniliforme* endoPG (1hg8.pdb) and *A. niger* endoPG ribbons (1czf.pdb). The arrow evidences the loop insertion between β 14 and β 15 of *F. moniliforme*.

highly represented. This was not the case for any of the endoPGs, even for *F. moniliforme* that displayed some affinity for methyl groups. Despite the combination of bioinformatics data and 3D modeling, it was very delicate to assess, either from the sequence alignment or from the cleft topology, the consensus motifs and residues responsible for their tolerance to methyl groups.

4. Discussion

4.1. Complex with un-methyl-esterified substrates

The docking of growing homogalacturonan provided a clear explanation for the action mode of *F. moniliforme* endoPG, either on the conformational behaviour of the homogalacturonan or on the cleavage pattern of the endoPG in correlation with the amino-acid residues that lined the subsites binding. The models may represent the Michaelis complexes in the reaction pathway, the step when the substrate binds to the cleft. The computational docking, performed for the first time on this enzyme, displayed a striking good agreement with previous experimental results performed on this enzyme [13]. Therefore, many structural and catalytic features, issued from previous crystallographic and modeling studies performed on other endoPGs, were confirmed except for the distortion of the 4C_1 chair of the GalA at subsite -1 [15,16,27]. The experiments showed that maximum velocity V_{\max} , strong affinity, and hydrolysis rate

increased with the length of the homogalacturonan chain, the modeling also evidenced a clear increase in the docking energy as the substrate was elongated. Besides, the asymmetric cleavage always occurred on the reducing side of the substrate. This distribution of the GalA residues, apart from the cleavage site, was in total agreement with the mass spectrometry results of the hydrolysis products [13,14]. The enzyme could bind up to six GalA moieties in its crevice, with a final subsite distribution from -4 to $+2$, evidencing subsite 4 for the first time (Fig. 4 (a), (b)). The solvent-accessible surface and the space-filling representation (Fig. 4 (a)) clearly showed that the middle part of the cleft was narrower and deeper to tightly bind the substrate while both ends were relatively wider, especially the end located at subsite $+2$. The non-reducing end of the substrate was directed toward the N-terminus of the enzyme. This docking scheme corroborates the crystallographic data and modeling studies on endopolygalacturonases of *A. aculeatus* and *S. purpureum* [15,27].

4.2. Subsites -1 and $+1$

The amino-acid residues involved in subsite binding have been clearly identified (Fig. 4(b)). They are labelled and coloured respectively in dark grey, purple, orange, magenta, red, and blue from subsites -4 to $+2$. As a matter of fact, the colours magenta, red, and yellow could be clustered around subsites -1 and $+1$ as the listed residues mostly participate to both subsites. Subsites -1 and $+1$ have one of the highest affinity for GalA. As catalytic subsites, it is not surprising that they displayed a very high affinity for the substrate. Similar affinity has already been demonstrated for *S. purpureum* PG [27]. We thus confirmed that eight amino-acid residues, strictly conserved in the polygalacturonase family, defined subsites -1 and $+1$ [15,27–29]. These include H188, N189, D191, D212, D213, H234, R267, and K269. All the residues are involved in the intricate hydrogen bonding networks that participate to the catalysis. As hypothesised for its equivalent D173 in *S. purpureum* [27], D212 could have also the appropriate position to be a proton donor for the fissile glycosidic bond. Its carboxylic group is the nearest to the glycosidic oxygen. D191 and D213 could be both candidates to act as a general base to abstract a proton from nucleophilic water. Besides, for each residue D191, D212, D213, R267, K269 except H234, a counterpart is present in the rhamnogalacturonase of *A. aculeatus* [15]. Such histidine residue could participate in substrate specificity.

Neither GalA at subsite -1 nor GalA at subsite $+1$ displayed any distortion from their conventional chair conformation. This contrasts with the distortion of the sugar located at subsite -1 that was evidenced in previous works [15,16]. It does not contrast with the crystallographic data of *E. chrysantemi* pectate lyase [32] where each of the four GalA rings were refined to a chair conformation with torsional angles closed to the ideal 2_1 or 3_1 native helices. From a catalytic point of view, this absence of deformation

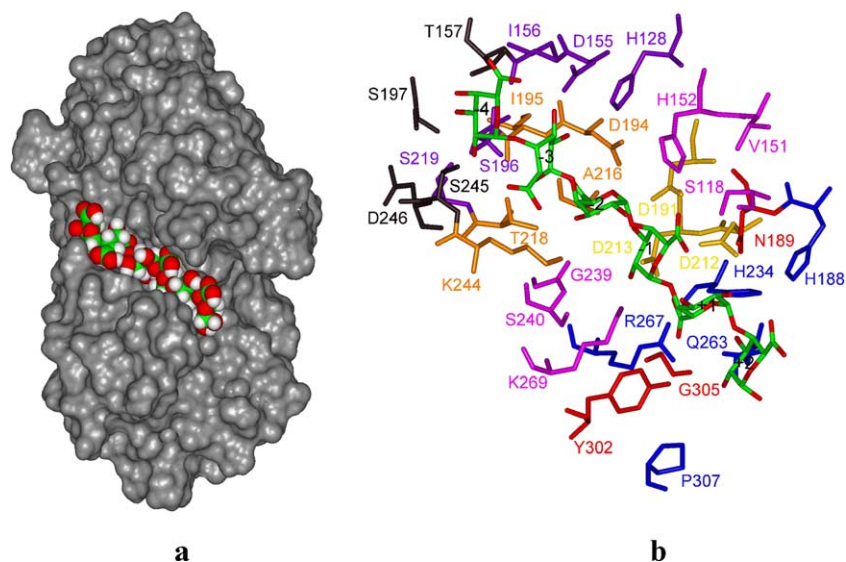


Fig. 4. (a) Modeled structure of endoPG complexed with a hexagalacturonate. The solvent accessible surface of the protein is drawn in grey and the substrate is represented in the space-filling model. The N-terminus is at the top and the C-terminus at the bottom. (b) The interaction between the protein and the hexagalacturonate (in stick and coloured by atom-type model) is detailed. The amino-acid residues involved in the binding subsites from -4 to $+2$ are respectively coloured in brown, purple, orange, magenta, red, and blue. The catalytic triad D191, D212, and D213 is coloured in yellow. (For interpretation of the references to colour in this figure legend, the reader is referred to the web version of this article.)

can be explained by the fact that we are in the early step of the Michaelis complex formation and not at the transition state. The amino-acid side chains were spatially conformed to avoid steric clash and to accommodate the incoming substrate. From a methodological approach, no constraint have been applied on the system and even Choi et al. mentioned a conversion from half-boat to chair forms when the artificial constraints are released [16].

4.3. Other subsites

Interestingly, subsite -3 displayed the highest affinity for sugar. For this reason, subsite -3 could be clearly suspected to drive the substrate into the crevice. K244, located between subsites -2 and -3 , could help the optimal positioning of the substrate above the catalytic triad. Its positive charge could actually monitor the binding of the group COO^- of GalA above -3 and thus favour the asymmetric cleavage. This electrostatic feature of the enzyme is in full accordance with its specificity suspected to be dictated by long-range electrostatic forces [19,31]. Subsite -3 involved the highest number of residues: H128, D155, T157, D194, S196, S219, K244, and S245. Among those residues, only three are conserved: respectively highly conserved for S219 and strictly conserved for D194 and S245. The 1D/3D alignment was done on *F. moniliforme*, *A. niger*, *A. aculeatus*, and *S. purpureum* endoPGs for which 3D structures were available (data not shown). At subsites -4 , -2 and $+2$, the GalA residues are bound through interactions located at both sides of the cleft as well. Subsites $+2$ and -2 display a rather strong and similar affinity for substrate. Subsite $+2$ involved H188, H234, Y302, G305, and P307 strictly conserved among the cited endoPGs, and Q263 not conserved at all.

Subsite -2 is composed of D194, I195, A216, T218, and K244 where only D194 and A216 are strictly conserved. For the first time, subsite -4 has been highlighted in this study as a fairly good binding site with a rather strong affinity value. It is composed of T157, S197, S245, and D246, where only S245 is conserved.

As a conclusion of this part, the main structural features of the homogalacturonan fragments as well as the action pattern of *F. moniliforme* endoPG, both determined experimentally, were confirmed and explained at a molecular resolution. This modeling study suggested that the binding cleft of *F. moniliforme* endoPG can tightly accommodate up to six GalA residues at subsites from -4 to $+2$. Subsite -5 or $+3$ would be exposed to solvent region and may not be shaped depending on the nearby amino-acid residues. Also, such distal subsites could have very weak binding affinity if they exist.

4.4. Complex with methyl-esterified substrates

Since our modeling work gave nice agreement with the experimental data on un-methyl-esterified substrates, the modeling computation with mono to highly methyl-esterified homogalacturonan fragments was expected to be predictive. The structural features, presented above, were confirmed with methyl-esterified substrates. Similarly, the binding energy increased with the length of the substrate and the asymmetric docking led to an asymmetric cleavage pattern. The protein energy and the docking energy values were globally within the same range compared to those measured previously. Variations up to 3 or 4 kcal/mol, alternating between reinforcement and decrease in docking, occurred when the methyl groups were docked at specific

subsites. Except for subsite –4, which gained up to 10 kcal/mol with the presence of a methyl group, each subsite displayed a similar binding strength when binding a methylesterified residue (Table 3). For all subsites, the identification of amino-acid residues was not changed with the presence of the methyl group.

4.5. Comparison with *A. niger* endoPGII

Even if many of the residues involved in subsite definition were found highly conserved, see (Figs. 4(b) and 5(b)), some differences could be relevant and specific for a comprehensive behaviour of the two enzymes towards substrate. In details between *F. moniliforme* and *A. niger*, subsite +1 is fully similar in both enzymes with strictly conserved residues. At subsite –1, the catalytic triad and the residues, G239, S240, and K269 residues are strictly conserved. S118 and V151 residues are replaced by I120 and L149 while H152 is aligned with M150. At subsite +2, the H188, H234, R267, and P307 residues are strictly conserved; only the Q263 residue is replaced by E252. At subsite –2, I195 is replaced by V184, T218 by N207, and K244 by R233. The main change lies in the chain length between K244 and R233. The latter is slightly longer than the former lysine residue and could prevent from the docking of a methyl group on this side of the cleft. At subsite –3, S219 and S245 are strictly conserved. In details, H128 is replaced by the longer K127, the acidic D155 is replaced by the polar S153, and the polar S196 is replaced by the small G185 with no lateral chain. Such differences with *F. moniliforme* could create endoPGII subsite –3 with less binding affinity for a methyl group at this position or in its vicinity (subsite –2 or –4). Finally, the main difference could occur at subsite –4. One should remember that subsite –4 is the only subsite that induced a noticeable

difference in docking energy towards methyl-esterified substrates. This subsite, with numerous serine residues S196, S197, S219, and S245 and isoleucine residues I156 and I195, could participate to the tolerance of *F. moniliforme* towards methylesterified substrates (Figs. 4(b) and 5(b)). Only S219 and S245 are conserved. I156 is replaced by V154, T157 by Q155, I195 is replaced by V184, S196 by G185, S197 by N186, and finally D246 by N235. This is the least conserved subsite.

4.6. Comparison with non-tolerant endoPGs and PME

A way to understand the difference in the docking of methylated or non-methylated substrates was to extend the comparison to enzymes known to display specific behaviour towards those pectins. EndoPGs with relevant difference towards methyl-esterified pectins were selected as well as pectate lyases and PMEs. Conversely to the first two, the latter are known to act specifically on the highly methyl-esterified pectins.

For a general trend, endoPGs, pectate lyases, and PMEs share a similar β fold with a conserved asparagine ladder and consensus motifs [27–32]. The 3D structures reveal main differences in loop lengths and hydrophobicity. The hydrophobic residues are highly represented in PMEs, where tryptophan, phenylalanine, and tyrosine residues are especially highly conserved at subsites –1 and +1. Those hydrophobic residues are strictly present in PMEs. They could actually be of tremendous help to position the apolar methyl groups above the catalytic subsites –1 and +1 and to reinforce the affinity for the enzyme. Despite those relevant features, bioinformatics and molecular visualisation failed to explain with certainty the tolerance towards methylesterified substrate.

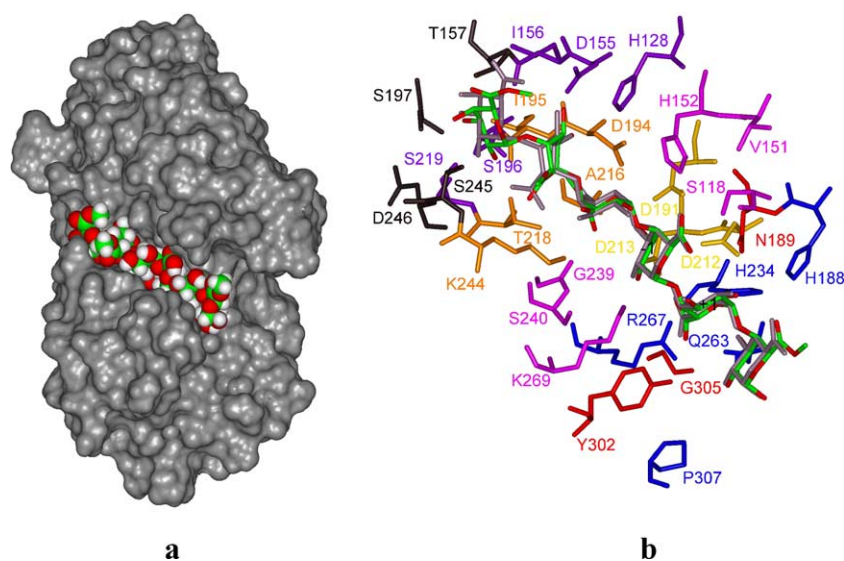


Fig. 5. (a) Modeled structure of endoPG complexed with a tetra-methylesterified hexagalacturonate. The solvent accessible surface of the protein is drawn in grey and the substrate is represented in space-filling model. (b) The interaction between the protein and the hexagalacturonate (in stick and coloured by atom-type model) is detailed. The previous DP6 with no methyl group is superimposed in grey. The same colour code is conserved for the amino-acid residues involved in the binding subsites from –4 to +2. No distortion from the ${}^4\text{C}_1$ chair for any of the sugar moieties can be noticed.

5. Conclusion

In this study, molecular modeling fully corroborated experimental results and gave molecular insights to the conformational behaviour of the homogalacturonan fragments within the active cleft of *F. moniliforme* endoPG. It quantitatively confirmed the experimental results with binding energy contributions and amino acid 3D identification. The study numbered the subsite optimum as six, ranging the accommodation of GalA from -4 to $+2$. Subsite -4 was evidenced for the first time. From that modeling, we understood the asymmetric binding mode of the homogalacturonan substrates and the catalytic consequences on the *F. moniliforme* endoPG cleavage pattern. From stretched tolerance of each subsite towards methylesterification, we were able to predict, with atomic details, the behaviour of mono and multi-methyl-esterified substrates inside the groove. The comparison with endoPGII from *A. niger* gave us clues to propose rational mutation points. It would be worth mutating K244R at subsite -3 or other residues at subsite -4 to get to a sequence more similar to *A. niger* and to test the consequences on the docking of methyl-esterified pectin fragments. Acetyl decorated and longer DP homogalacturonan fragments are now ready for future computational modeling and complete understanding of the degradation of smooth regions of pectins by *F. moniliforme* endopolygalacturonase.

References

- [1] H. Neukom, Über den Abbau von Pektinstoffen, Schweiz. Landwirtsch. Forsch. 2 (1963) 112–122.
- [2] W.M. Fogarty, C.T. Kelly, Pectic Enzymes, Microbial Enzymes and Biotechnology, Applied Science Publishers, London, UK, 1983, pp. 131–182.
- [3] T. Sakai, T. Sakamoto, J. Hallaert, E.J. Vandamme, Pectin, pectinase and protopectinase: production, properties and applications, Adv. Appl. Microbiol. 39 (1993) 213–294.
- [4] C. Lang, H. Dönenburg, Perspectives in the biological function and the technological application of polygalacturonases, Appl. Microbiol. Biotechnol. 53 (2000) 366–375.
- [5] B. Henrissat, G.J. Davies, Structural and sequence-based classification of glycoside hydrolases, Curr. Opin. Struct. Biol. 7 (1997) 637–644.
- [6] B. Henrissat, Enzymology of cell-wall degradation, Biochem. Soc. Trans. 26 (1998) 153–156.
- [7] E.M.W. Chen, A.J. Mort, Nature of sites hydrolyzable by endopolygalacturonase in partially-esterified homogalacturonans, Carbohydr. Polym. 29 (1996) 129–136.
- [8] J.A.E. Benen, H.C.M. Kester, J. Visser, Kinetic characterization of *Aspergillus niger* N400 endopolygalacturonases I, II and C, Eur. J. Biochem. 259 (1999) 577–585.
- [9] L. Parenicova, J.A.E. Benen, H. Kester, J. Visser, endoPGaA and endoPGaB encode two constitutively expressed endopolygalacturonases of *Aspergillus niger*, Biochem. J. 345 (2000) 637–644.
- [10] L. Parenicova, H.C.M. Kester, J.A.E. Benen, J. Visser, Characterization of a novel endopolygalacturonase from *Aspergillus niger* with unique kinetic properties, FEBS Lett. 467 (2000) 333–336.
- [11] P.W. Talboys, Damage, symptoms and crop loss caused by vascular pathogens, in: R.K.A. Wood, G.J. Jellis (Eds.), Plant Diseases: Infection, Damage and Loss, Blackwell Scientific Publications, Oxford, 1984, pp. 171–187.
- [12] L.-K. Huang, R.R. Mahoney, Purification and characterization of an endo-polygalacturonase from *Verticillium albo-atrum*, J. Appl. Microbiol. 86 (1999) 145–156.
- [13] E. Bonnin, A. Le Goff, R. Körner, G.J.W.M. van Alebeek, T.M.I.E. Christensen, A.G.J. Voragen, P. Roepstorff, A. Caprari, J.-F. Thibault, Study of the mode of action of endopolygalacturonase from *Fusarium moniliforme*, Biochim. Biophys. Acta 1526 (2001) 301–309.
- [14] E. Bonnin, A. Le Goff, R. Körner, J. Vigouroux, P. Roepstorff, J.-F. Thibault, Hydrolysis of pectins with different degrees and patterns of methylation by the endopolygalacturonase of *Fusarium moniliforme*, Biochim. Biophys. Acta 1596 (2002) 83–94.
- [15] S.W. Cho, S. Lee, W. Shin, The X-ray structure of *Aspergillus aculeatus* Polygalacturonase and a modeled structure of the polygalacturonase–octagalacturonate complex, J. Mol. Biol. 314 (2001) 863–878.
- [16] J.K. Choi, B.H. Lee, C.H. Chae, W. Shin, Computer modeling of the rhamnogalacturonase–“hairy” pectin complex, proteins, Struct. Funct. Bioinformatics 55 (2004) 22–33.
- [17] G. André, A. Buléon, M. Juy, N. Aghajari, R. Haser, V. Tran, Amylose chain behavior in an interacting context II—molecular modelling of a maltopentaose fragment in the barley α -amylase catalytic site, Biopolymers 49 (1999) 107–119.
- [18] G. André, A. Buléon, R. Haser, V. Tran, Amylose chain behaviour in an interacting context III—complete occupancy of the AMY2 barley α -amylase cleft and comparison with biochemical data, Biopolymers 50 (1999) 751–762.
- [19] L. Federici, C. Caprari, B. Mattei, C. Savino, A. Di Matteo, G. De Lorenzo, F. Cervone, D. Tsernoglou, Structural requirements of endopolygalacturonase for the interaction with endoPGIP (polygalacturonase-inhibiting protein), Proc. Natl. Acad. Sci. U. S. A. 98 (2001) 13425–13430.
- [20] C. Dodge, R. Schneider, C. Sander, The HSSP database of protein structure–sequence alignments and family profiles, Nucleic Acids Res. 26 (1998) 313–315.
- [21] E.M. Zdobnov, R. Lopez, R. Apweiler, T. Etzold, The EBI SRS server—recent developments, Bioinformatics 18 (2002) 368–373.
- [22] O. Poirot, K. Suhre, C. Abergel, E. O’Toole, C. Notredame, 3DCoffee: a web server for mixing sequences and structures into multiple sequence alignments, Nucleic Acids Res. 32 (2004) 37–40.
- [23] I. Jonassen, J.-F. Collins, D. Higgins, Finding flexible patterns in unaligned protein sequences, Protein Sci. 4 (1995) 1587–1595.
- [24] A. Di Nola, G. Fabrizi, D. Lamba, L. Segre, Solution conformation of a pectic acid fragment by 1H-NMR and molecular dynamics, Biopolymers 34 (1994) 457–462.
- [25] M.D. Walknshaw, S. Arnott, Conformations and interactions of pectins—I X-ray diffraction analyses of sodium pectate in neutral and acidified forms, J. Mol. Biol. 153 (1981) 1055–1073.
- [26] S. Cros, C. Hervé du Penhoat, N. Bouchemal, H. Ohassan, A. Imbert, S. Pérez, Solution conformation of a pectin fragment disaccharide using molecular modelling and nuclear magnetic resonance, Int. J. Biol. Macromol. 14 (1992) 313–320.
- [27] T. Shimizu, T. Nakatsu, K. Miyairi, T. Okuno, H. Kato, Active-site architecture of endopolygalacturonase I from *Stereum purpureum* revealed by crystal structures in native and ligand-bound forms at atomic resolution, Biochemistry 41 (2002) 6651–6659.
- [28] Y. Van Santen, J.A.E. Benen, K.-H. Schroter, K.H. Kalk, S. Armand, J. Visser, B.W. Dijkstra, 1.68 Å crystal structure of endopolygalacturonase II from *Aspergillus Niger* and identification of active site residues by site-directed mutagenesis, J. Biol. Chem. 274 (1999) 30474–30480.
- [29] S. Armand, M.J.M. Wagemaker, P. Sanchez-Torres, H.C.M. Kester, Y. van Santen, B.W. Dijkstra, J. Visser, J.A.E. Benen, The active site topology of *Aspergillus niger* endopolygalacturonase II as studied by site-directed mutagenesis, J. Biol. Chem. 275 (2000) 691–696.
- [30] R.D. Scavetta, S.R. Herron, A.T. Hotchkiss, N. Kita, N.T. Keen, J.A.E. Benen, H.C.M. Kester, J. Visser, F. Jurnak, Structure of a plant

- cell wall fragment complexed to pectate lyase C, *Plant Cell* 11 (1999) 1081–1092.
- [31] O. Mayans, M. Scott, I. Connerton, T. Gravesen, J. Benen, J. Visser, R. Pickersgill, J. Jenkins, Two crystal structures of pectin lyase A from *Aspergillus* reveal a pH driven conformational change and striking divergence in the substrate-binding clefts of pectin and pectate lyases, *Structure* 5 (1997) 677–689.
- [32] J. Jenkins, O. Mayans, D. Smith, K. Worboys, R.W. Pickersgill, Three-dimensional structure of *Erwinia chrysantemi* pectin methyl-esterase reveals a novel esterase active site, *J. Mol. Biol.* 305 (2001) 951–960.
- [33] P. Gouet, E. Courcelle, D.I. Stuart, F. Metoz, ESPript: multiple sequence alignments in PostScript, *Bioinformatics* 15 (1999) 305–308.